Particulate Emission Reduction in Small-Scale Biomass Combustion Plants by a Condensing Heat Exchanger

C. J. J. M. de Best,[†,‡] H. P. van Kemenade,[*,†] T. Brunner,[†,‡] and I. Obernberger[†,‡]

Faculty of Mechanical Engineering, Division Thermo Fluids Engineering, Technische Universiteit Eindhoven, Post Office Box 513, 5600 MB Eindhoven, The Netherlands, and Austrian Bioenergy Centre GmbH, Inffeldgasse 21b, A-8010 Graz, Austria

Received August 28, 2006. Revised Manuscript Received May 2, 2007

Use of biomass fuels for energy purposes has gained increasing importance as a method to reduce greenhouse gas emissions. In comparison to gaseous and liquid fossil fuels, the emissions of particulate matter are higher, leading to concerns about the availability of cost-effective techniques to reduce aerosol emissions in small-scale biomass combustion plants. In this work, the applicability of reducing aerosol emissions by stimulating condensation of aerosol-forming vapors on the heat-exchanger furnaces is investigated. A first-order estimation indicates that the heat-exchanger passage has to be in the order of millimeters to obtain a higher wall condensation rate compared to heterogeneous condensation, a result verified with purpose-built heat exchangers connected to a grate furnace. The measurements show that heat exchangers with an equivalent tube diameter of approximately 2 mm can reduce the aerosol emissions by approximately 70% compared to conventional boiler designs.

1. Introduction

Worldwide there is a growing interest in the use of biomass fuels for energy production purposes. Bioenergy is seen as one of the options to mitigate greenhouse gas emissions and substitute fossil fuels.[9] In comparison to liquid and gaseous fuels, the emissions of particulate matter are high, and considering the health risks,[2] methods to reduce aerosol emissions have to be implemented even in small-scale biomass-fired units.

The particle size distribution of particles formed during biomass combustion can be divided into a coarse mode, the coarse fly ash fraction, and a fine mode, the aerosols. The first fraction consists of coarse fly ash particles entrained from the fuel bed. This ash fraction increases with the boiler load because of higher flue gas velocities and is strongly dependent upon the combustion technology, the design of the combustion unit, and the process control system used.[4] The particle size of coarse fly ash emissions can vary between a few micrometers up to about 200 μm. The second fraction consists of aerosols, formed during the cooling of the flue gas in the heat-exchanger section. During combustion, volatile aerosol-forming elements (e.g., K, Cl, S, Pb, Na, and Zn) are easily released from the fuel to the gas phase and subsequently undergo chemical reaction. They form, for instance, KCl and K_2SO_4. Almost no significant release of Si, Mg, and Ca is observed.[5,10] As soon as the concentration of these aerosol-forming vapors in the flue gas and the cooling rate in the heat exchanger are high enough, supersaturation of these vapors could occur, causing the formation of particles by nucleation. The particles formed by nucleation are very small in size, about 5−10 nm, but on their way with the flue gas, these particles are able to grow by coagulation, agglomeration, and condensation of aerosol-forming vapors on their surfaces.[4,7,15,17,18,23] These particles form the major part of the aerosol fraction, characterized by a particle size < 1 μm.

2. Objectives

Coarse fly ash particles can be removed cost-efficiently using cyclones or multicyclones.[3,4] Baghouse filters or electrostatistic precipitators, as used in large-scale biomass combustion plants to precipiate aerosol particles from the flue gas, are presently from an economic point of view not suitable in small-scale combustion units.[8] Therefore, a cost-efficient technique has to be developed that specially aims at the reduction of aerosol emissions in small-scale biomass combustion units.

The objective of this paper is to investigate the feasibility of designing a heat exchanger wherein condensation of the vapors

* To whom correspondence should be addressed. Telephone: +31-40-247-3156. Fax: +31-40-247-5399. E-mail: h.p.v.kemenade@tue.nl.

† Technische Universiteit Eindhoven.

‡ Austrian Bioenergy Centre GmbH.

(1) Bird, R. B.; Steward, W. E.; Lightfoot, E. N. *Transport Phenomena*, 2nd ed.; John Wiley and Sons, Inc.: New York, 2002; ISBN 0-471-41077-2.

(2) Braun-Fahrländer, C. In Proceedings of the IEA Seminar Aerosols from Biomass Combustion; Nussbaumer, T., Ed.; Verenum: Zürich, Switserland, 2001; pp 11–18.

(3) Brouwers, J. J. H. *Powder Technol.* **1997**, *92* (2), 89–99.

(4) Brunner, T.; Obernberger, I.; Brouwers, J. J. H.; Preveden, Z. In Proceedings of the 10th European Bioenergy Conference; Würzburg, A. A., Ed.; Germany, 1998; pp 1630–1633.

(5) Brunner, T.; Jöller, M.; Obernberger, I.; Frandsen, F. In 12th European Conference and Technology Exhibition on Biomass for Energy, Industry, and Climate Protection, Amsterdam, The Netherlands, August 2002.

(6) Brunner, T. Aerosols and coarse fly ashes in fixed-bed biomass combustion plants—Formation, characterisation and emissions. Ph.D. Thesis, Department of Mechanical Engineering, Technische Universiteit Eindhoven, Graz, Austria, 2006; ISBN 3-650 1980 3-2.

(7) Christensen, K. A.; Stenholm, M.; Livbjerg, H. *J. Aerosol Sci.* **1998**, *29* (4), 421–444.

(8) Ebert, F. In Proceedings of the IEA Seminar Aerosols from Biomass Combustion; Nussbaumer, T., Ed.; Verenum: Zürich, Switserland, 2001; pp 41–46.

(9) Faaij, A. P. C. *Energy Policy* **2006**, *34*, 322–342.

(10) Frandsen, F. J.; Moiraghi, L.; van Lith S.; Jensen, A. J.; Glarborg, P. In *Aerosol in Biomass Combustion*; Obernberger, I., Ed.; Medienfabrik Graz: Graz, Austria, 2005; pp 65–77.

10.1021/ef060435t CCC: $37.00

Published on Web 12/21/2007

directly on the heat-exchanger surface is stimulated to reduce particle formation and emissions. Therefore, in section 3, a first-order estimation of the competing mechanisms of wall condensation and heterogeneous condensation in a heat-exchanger passage is made to provide guidelines for the dimensioning of a condensing heat exchanger. On the basis of these guidelines, prototype heat exchangers are designed and tested.

Within the European Union (EU) project BIOAEROSOLS (ERK6-CT1999-0003), an aerosol formation model originally developed by Christensen[7] was analyzed to obtain insights into the particle formation process in biomass combustion plants. The model is based on a well-stirred reactor model including particle formation and growth mechanisms. The model consistently overpredicted the amount of aerosols formed compared to the results of an extensive measurement campaign. The reason for this deviation was mainly caused by overestimating the amount of aerosol-forming elements released from the fuel to the gas phase. One of the conclusions was that that aerosols are mainly formed because of heterogeneous condensation or homogeneous nucleation during the cooling of the flue gas in the heat-exchanger passage.

van Kemenade[20] derived a model to investigate which mechanisms cause particle deposition in conventional boiler designs. The model derived includes transport mechanisms of both particles and aerosol-forming vapors. It has been shown that, from wall deposition mechanisms, such as thermophoresis, Brownian diffusion, eddy impactation, and direct wall condensation, only wall condensation had a significant impact on the aerosol emission reduction. Further analysis showed that the designs of the boilers are such that within the limits of the applications wall condensation is minimal, as is expected to minimize fouling of the heat-exchanger surfaces. However, small-scale installations might benefit from a heat exchanger that stimulates wall condensation as a mechanism to reduce aerosol formation provided that a cleaning system for the fouling layer can be devised.

3. Heterogeneous Condensation versus Wall Condensation

As soon as the flue gas temperature equals the condensation temperature of aerosol-forming species in a heat exchanger, condensation on pre-existing particles as well as on heat-exchanger walls takes place as competing processes. To make a first-order estimation of the amount of vapor that condenses on the walls of a heat exchanger, it is assumed that both the nuclei in the gas and the walls of the heat exchanger are below the condensation temperature of the aerosol-forming vapors. In that case, the vapor molecules diffuse both to the wall and the aerosol particles. To simplify the calculations regarding the condensation rate on particles and heat-exchanger walls, it is assumed that the number concentration of aerosol particles near the heat-exchanger inlet and during the cooling process are constant.

From measurements, it is known that a rather constant aerosol number concentration downstream of hot-water boilers can be observed, which is usually in the order of 1×10^{13} N m^{-3} (see Brunner).[5] It is expected that the number concentration of aerosols during the cooling process does not change significantly, which implies that the number concentration of aerosols near the heat-exchanger inlet is also within the same range. The reason for this constant number concentration can be awarded to coagulation processes. ZnO particles for instance are assumed to form in large amounts directly after the flue gases leave the fuel bed.[6] On their way with the flue gas, these particle are able to coagulate. The final number concentration when the aerosol particles enter the heat-exchanger inlet mainly depend upon the initial number concentration and the time available. To illustrate this coagulation process, a simple monodisperse coagulation model is used to predict the number concentration as a function of time. The time-dependent coagulation process is given by Hinds[12]

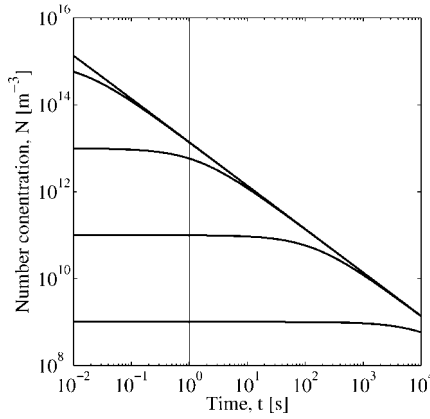

Figure 1. Logarithmic representation of a simple monodisperse coagulation model. The coagulation coefficient K_0 is evaluated at a flue gas temperature of 1000 °C. The horizontal axis represents the time t, whereas the vertical axis represents the number concentration N.

$$N(t) = \frac{N_0}{1 + N_0 K_0 t} \tag{1}$$

where N_0 represents the initial number concentration, K_0 is the coagulation coefficient, and t represents the time. The coagulation coefficient is determined at a typical flue gas temperature of 1000 °C.

Figure 1 shows a graphical representation of the number concentration decrease for various initial number concentrations. Assuming a typical residence time of the flue gas inside the furnace in the order of some seconds indicates that the number concentration near the heat-exchanger inlet is always within the range of 1×10^{13} N m^{-3}, which is a conservative approximation. Because the time required for further coagulation increases exponentially, it is unlikely that the aerosol number concentration in the heat exchanger itself decreases significantly, especially taken into account that the residence time inside the heat exchanger (therefore, the time available for coagulation) is also limited to at maximum of a couple seconds. Furthermore, it is assumed that particle formation by nucleation as described in Christensen[7] is widely suppressed because of the high aerosol concentration near the heat-exchanger inlet and could therefore be excluded in the first analysis.

To estimate the wall condensation rate, a laminar flow in an axis-symmetric heat-exchanger tube is assumed, which is characterized by a Reynolds number lower than 2300[1]

$$\mathrm{Re} = \frac{D_{\mathrm{eq}} \rho_{\mathrm{g}} V_{\mathrm{g}}}{\mu_{\mathrm{g}}} < 2300 \tag{2}$$

In eq 2, D_{eq} represents the equivalent diameter of one heat-exchanger tube, which is defined as $4A/O$, where A represents

(11) Fuchs, N. A. *The Mechanics of Aerosols*; Pergamon Press Ltd.: New York, 1964; ISBN 0-471-41077-2.
(12) Hinds, W. C. *Aerosol Technology*; John Wiley and Sons, Inc.: New York, 1982.
(13) Janna, W. S. *Engineering Heat Transfer*, 2nd ed.; CRC Press: Boca Raton, FL, 2000.

the cross-section of the conduit and O is the wetted perimeter. ρ_g and μ_g represent the density and dynamic viscosity of the flue gas, respectively, whereas V_g represents the axial bulk velocity of the flue gas.

The mass vapor flux toward the walls of the heat exchanger per unit length $j'_{a,w}$ can be written as (Bird et al.[1])

$$j'_{a,w} = \frac{\mathrm{Sh}(D_{eq})\pi \mathbf{D} M_a}{R_u T_g}(p_{a,w} - p_{a,g}) \tag{3}$$

where M_a represents the molar mass of the aerosol-forming vapor elements, R_u is the universal gas constant, T_g is the flue gas temperature, p is the partial vapor pressure, whereas **D** represents the diffusion coefficient of the aerosol-forming vapors. The subscript a refers to the aerosol-forming vapor element, whereas the subscripts w and g refers to its position, respectively, on the wall of the heat exchanger and relatively far away from the wall in the bulk of the flue gas. In eq 3, $\mathrm{Sh}(D_{eq})$ represents the Sherwood number, which is a dimensionless number to calculate the mass-transfer rate. This number represents the ratio of the length scale (in this case, the equivalent tube diameter, D_{eq}) to the diffuse boundary layer thickness. Because a fully developed laminar flow is assumed, the Sherwood number is constant at 3.66 when applying a constant wall temperature (Bird et al.[1]).

A similar relation as described in eq 3 but now for the vapor flux toward the particles in the tube per unit length is derived. The total particle surface area in a tube per unit length $A'p$ is defined as

$$A'_p = \pi d_p^2 N \frac{\pi}{4} D_{eq}^2 \tag{4}$$

where the term πd_p^2 represents the surface area of one nucleus and N represents the number of nuclei per cubic meter, whereas $^{\pi}\backslash_4 D_{eq}^2$ represents the volume per unit length. Therefore, the vapor flux toward the particles in the tube per unit length can be defined as

$$j'_{a,p} = \frac{N d_p \mathrm{Sh}(d_p)\varphi \pi^2 D_{eq}^2 \mathbf{D} M_a}{4 R_u T_g}(p_{a,p} - p_{a,g}) \tag{5}$$

Equation 5 is based on the diffusion of molecules to the surface of the particle in the continuum limit. A correction factor φ for diffusion outside the continuum regime is introduced, while the dimensions of the particles are within the mean free path regime. In that case, transport is controlled by kinetic processes. The effect of the correction factor φ results in a slowing down of the growth rate and is given by the Dahneke equation (Seinfeld[19])

$$\varphi(\mathrm{Kn}_d) = \frac{1 + \mathrm{Kn}_d}{1 + 2\mathrm{Kn}_d(1 + \mathrm{Kn}_d)} \tag{6}$$

where Kn_d is given by

$$\mathrm{Kn}_d = \frac{4\mathbf{D}}{d_p}\left(\frac{\pi M_a}{8 R_u T_g}\right)^{\frac{1}{2}} \tag{7}$$

Inertia effects can be neglected for particles in the submicrometer range (Fuchs[11]), implying that the particles follow the streamlines and the net flow around the particle is zero. Therefore, the Sherwood number $\mathrm{Sh}(d_p)$ as mentioned in eq 5 equals 2 in the case of small net mass-transfer rates, and there is zero flow around a spherical particle.

In eq 5, it is assumed that the particle temperature equals the flue gas temperature. However for a particle in a condensing atmosphere, particle heating takes place because of the release of latent heat of vaporization during the condensation process. An equilibrium particle temperature is established when the energy necessary to heat up the particle is in balance with the heat loss as a result of conduction to the surrounding flue gas. The resulting quasi-static temperature between the particle and surrounding flue gas $T_p - T_g$ is given by Hinds[12]

$$T_p - T_g = \frac{\mathbf{D} M_a L \varphi}{R_u k_g}\left(\frac{p_{a,p}}{T_p} - \frac{p_{a,g}}{T_g}\right) \tag{8}$$

where k_g is the thermal conductivity of the surrounding flue gas. Assuming that potassium sulfate K_2SO_4 is the main aerosol-forming element, then L represents the latent heat of vaporization of K_2SO_4. Because of the temperature dependency of the saturation pressure at the particle interface $P_{a,p}$ and the particle temperature itself T_p, eq 8 cannot be solved explicitly. Because of this, eq 8 is solved numerically. For the calculations, a particle diameter d_p of typically 0.1 μm is assumed to calculate the correction factor φ. Figure 2 shows a graphical representation of $T_p - T_g$ for various flue gas temperatures as a function of the saturation ratio S, assuming that K_2SO_4 is the main aerosol-forming element. This saturation ratio, which is the ratio of the actual partial vapor pressure of the vapor in the flue gas to the saturation vapor pressure based on the flue gas temperature is defined as (Hinds[12])

$$S = \frac{p_{a,g}}{p_{a,sat}} \tag{9}$$

where $p_{a,g}$ represents the actual partial vapor pressure in the flue gas, whereas $p_{a,sat}$ represents the saturation vapor pressure evaluated on the flue gas temperature.

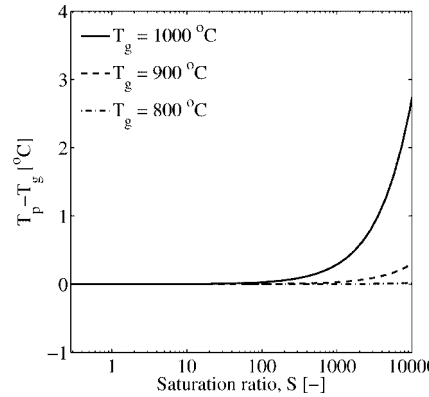

Figure 2. Particle temperature minus flue gas temperature $T_p - T_g$ versus the saturation ratio S for flue gas temperatures of 800−1000 °C. Simulations are performed under the assumption that K_2SO_4 is the main aerosol-forming element. The size of the particle during the simulation was always 0.1 μm.

From Figure 2, it can be observed that the difference between the particle temperature and flue gas temperature is dependent upon the flue gas temperature itself and the degree of saturation. During the growth process, the effect of the rising particle temperature results in an increase of the partial vapor pressure near the surface of the particle, which results in a slowing down of the net condensational growth rate. Because of this, the temperature difference between the particle temperature and the surrounding flue gas is relatively small for a wide range of saturation ratios. A quantitative approach in the case of applying a saturation ratio of 10 000 (which is extremely high) and a flue gas temperature of 1000 °C, results in a temperature difference $T_p - T_g$ of less than 3 °C, whereas the temperature difference for the same saturation ratio in the case of applying a flue gas temperature of 800 °C results in an insignificant

temperature difference between the particle temperature and surrounding flue gas temperature. Therefore, the assumption that the particle temperature equals the flue gas temperature for a wide range of flue gas temperatures as well as for a wide range of saturation ratios is a reasonable approach because of the relatively small resulting temperature differences.

If wall condensation and heterogeneous condensation take place at the same moment and all other particle deposition mechanisms are neglected, the absolute wall condensation rate $\epsilon_{abs,theo}$ can be expressed as the ratio of the vapor flux toward the walls compared to the total vapor flux per unit length

$$\epsilon_{abs,theo} = \frac{j'_{a,w}}{j'_{a,w} + j'_{a,w}} \tag{10}$$

Using the fact that the particle temperature equals the flue gas temperature indicates that $p_{a,p}$ equals the saturation pressure evaluated at the flue gas temperature, $p_{a,sat}$. Furthermore, the wall saturation ratio, S_{wall}, is introduced and is defined as

$$S_w = \frac{p_{a,w}}{p_{a,sat}} \tag{11}$$

Substituting eqs 3, 5, 9, and 11 into eq 10 and applying the previous described assumptions yields the following expression for the absolute wall condensation rate

$$\epsilon_{abs,theo} = \frac{\mathrm{Sh}(D_{eq})(S_w - S)}{\mathrm{Sh}(D_{eq})(S_w - S) + \frac{\pi}{4} D_{eq}^2 \varphi \mathrm{Sh}(d_p) N d_p (1 - S)} \tag{12}$$

In eq 12, S_w is strongly dependent upon the wall temperature of the heat exchanger, which is always below the bulk temperature of the flue gas. This implies that, because of the strong temperature dependency of the vapor pressure of the aerosol-forming elements, the vapor pressure of the aerosol-forming elements near the wall of a heat exchanger $p_{a,w}$ is always lower than the vapor pressure of the aerosol-forming elements in the bulk of the flue gas. Therefore, S_w is always smaller than 1. The other way around indicates that the saturation ratio of the aerosol-forming elements in the bulk of the flue gas is always significantly larger than 1 when assuming K_2SO_4 as the main aerosol-forming element to establish particle condensation.

From eq 12, it can be observed that the absolute wall condensation rate is strongly dependent upon the saturation ratio in the bulk S and near the wall S_w. Before investigating the influence of the saturation ratio S on the total wall condensation rate, first the wall saturation ratio has to be determined. In the case of a water-cooled heat exchanger, it is assumed that the wall temperature of the heat exchanger equals the water temperature, which is much smaller than the flue gas temperature. Consequently, the wall saturation ratio S_w in the region where wall condensation occurs goes to zero because of the strong temperature dependency of the saturation pressure of the aerosol-forming species. In other words, when $S_w \ll 1$, the contribution of S_w can be neglected and eq 12 is only dependent upon the saturation ratio S. This situation changes in the case that the wall temperature is slightly below the flue gas temperature, for instance, when applying a gas to the gas heat exchanger. However, the difference in the wall condensation ratio for applying a wall saturation ratio $S_w \approx 0.5$ instead of an wall condensation ratio $S_w = 0$ is less than 10% when a saturation ratio $S = 1.5$ is assumed. Increasing the saturation ratio S rapidly indicates that the influence of S_w could be neglected. Because of this, several simulations have been performed for various saturation ratios S under the assumption that $S_w = 0$ (see Figure 3).

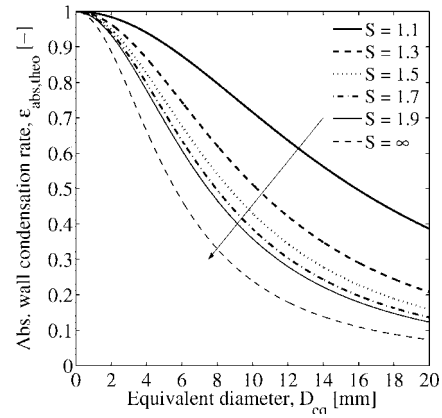

Figure 3. Effect of the tube diameter D_{eq} on the absolute wall condensation rate, $\epsilon_{abs,theo}$ for various saturation ratios. Initial conditions: $N = 10^{-13}$ m^{-3} μm, and $S_w = 0$.

From Figure 3, two effects regarding the wall condensation rate can be observed. First of all, decreasing the tube diameter down to typically 2 mm results in a significant increase of the wall condensation rate for all saturation ratios S. Consequently, decreasing the tube diameter results in a significant decrease of the particulate emissions at the heat-exchanger outlet, which is the desired effect. Increasing the diameter indicates that condensation of aerosol-forming vapors on pre-existing surfaces (particles) rapidly becomes the dominating process, thus increasing the particle mass emitted. Theoretically, an absolute wall condensation rate up to almost 90% can be achieved by applying a tube diameter of approximately 2 mm. In principle, also decreasing the saturation ratio slightly above 1 can result in a higher wall condensation ratio for large tube diameters. Theoretically, a wall condensation rate of 100% could be achieved in the limit when S goes to 1. This means that there is no net cooling rate or driving force for condensation because of the fact that the wall saturation ratio S_w equals S, making this solution impractical.

4. Experimental Setup

To assess the practical applicability of heat exchangers with small dimensions in biomass combustion, experiments were conducted using a pilot-scale biomass combustion plant with a nominal capacity of 180 kW_{th}. In the following section, the biomass combustion plant, the different heat exchangers applied, as well as the testing procedure are described.

4.1. Biomass Combustion Plant. The biomass combustion plant itself consists of a furnace equipped with a horizontally moving grate, staged air injection, and a flame tube boiler comprising a fire tube and two ducts of flame tubes with an inner diameter of $1^1\backslash_2$ in. (see Figure 4). The first and second ducts of the flame tube boiler are equipped with 30 and 16 tubes, respectively. Furnace temperatures are measured continuously in several zones and are controlled by flue gas recirculation below and above the grate. The nominal boiler capacity amounts to 180 kW_{th}.

The heat exchangers tested were connected with the secondary combustion zone via a slip stream (see Figure 4). One test heat exchanger itself can easily be replaced by another one; therefore, a flexible experimental setup was realized. The flow through the heat exchanger and the measurement section was established by a flue gas fan. The flue gas velocity in the test heat exchanger and measurement section is controlled manually, whereas a computer-controlled flue gas fan is used after the boiler. The measurement section after the test heat exchanger consists of a $1^1\backslash_4$ in. tube. Devices for measuring the flue gas temperature, velocity, oxygen content, and particulate emissions are mentioned in this section, denoted with T, V, O_2, and BLPI, respectively (see Figure 4). The same measurement devices are also mounted in the flue gas duct

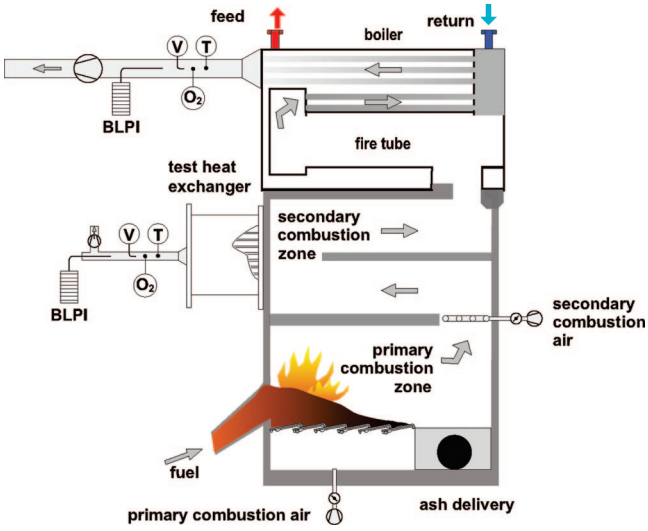

Figure 4. Experimental setup of the biomass combustion plant with measurement points after both the test heat exchanger and boiler.

after the boiler (see Figure 4). Type K thermocouples were used to measure the temperatures, whereas Prandtl tubes were used for measuring the flue gas velocities. A data acquisition system is used to sample all data continuously. Nine-stage Berner-type low-pressure impactors (BLPIs) and upstream nozzles for isokinetic sampling are used for measuring the particulate emissions downstream of the test heat exchangers as well as downstream of the boiler. While the previously mentioned measuring devices are working continuously, the impactors are noncontinuous measurement devices.

4.2. Heat Exchangers. Commonly used fire tube boilers operate in the turbulent regime to obtain a higher heat-transfer coefficient. Increasing the Reynolds number results in an increase of the convective heat transfer between the walls of the heat exchanger and the bulk of the flow but causes a high pressure drop and, consequently, requires a lot of energy.[13] Contrary to turbulent flow heat exchangers, laminar flow heat exchangers (Re < 2300) are based on conductive heat transfer, which cause a lower pressure drop but require a larger heat-exchanging surface. The volume and amount of material used can be kept in the same order by decreasing the size of the channels, thus maintaining structural integrity while increasing the heat-exchanging surface.

From Figure 12, the need to reduce the tube diameter into the millimeter regime can be observed to reduce the particulate emissions by enhancing wall condensation. Reducing the tube diameter automatically results in a laminar flow behavior. On the basis of this theory, three laminar flow heat exchangers with different dimensions were designed to measure the influence of the tube diameter on the particulate reduction. The boundary conditions, concerning the design of these exchangers, are derived from physical and practical limitations: (1) The Reynolds number based on the flue gas velocity inside the heat exchanger should always be below 2300 to achieve a laminar flow. (2) The flue gas temperature after the heat exchanger should be less than 200 °C to make sure that the condensation process of all volatilized species in the flue gas is fully completed and to achieve a reasonable thermal efficiency. In this way, a comparison of the particulate reduction with common boiler designs is permitted. (3) The pressure drop over the heat exchanger should be less than 350 Pa and, therefore, be comparable with usually applied boiler designs. (4) A minimum flue gas velocity of 6 m/s in the measurement section is required to perform accurate BLPI measurements.

Two laminar flow shell and tube water-cooled heat exchangers and one compact laminar counterflow gas to gas heat exchanger were designed for the experiments. In the next sections, the heat exchangers are discussed in more detail.

4.2.1. Laminar Flow Shell and Tube Heat Exchanger. A shell and tube heat exchanger with a variable inner tube diameter was developed on the basis of the previously mentioned boundary

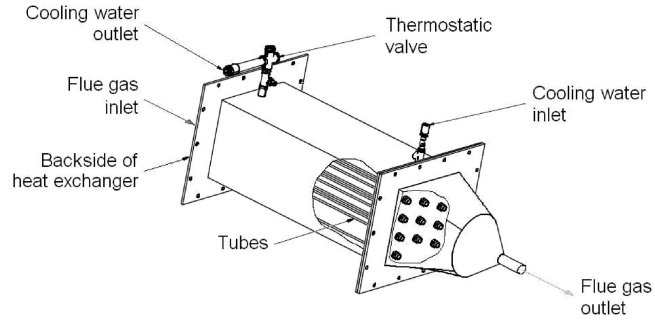

Figure 5. Schematic picture of the shell and tube heat exchanger.

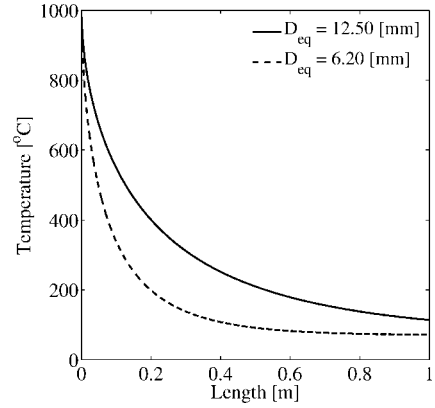

Figure 6. Calculated flue gas temperature for two different tube dimensions as a function of the length for the water-cooled heat exchanger.

conditions (see Figure 5). Water flows around the circular tubes. A total of 5 or 15 tubes for tube diameters of 12.50 and 6.20 mm, respectively, are used for the experiments. A thermostatic valve near the cooling water outlet was used to control the water temperature by flow regulation. The tubes inside the heat exchanger have a fixed length of 1 m and can easily be exchanged by tubes with other diameters. The side of the heat exchanger, which is directly in contact with the flue gas, is covered with a heat-resistance insulation plate. This insulation plate minimizes the temperature drop of the flue gas in front of the inlet of the heat exchanger because of radiation. When the inlet temperature of the flue gas is below the condensation temperature of the aerosol-forming species, condensation can already occur in front of the heat exchanger, instead of inside the heat exchanger, which is an undesirable effect.

For the calculations, the wall temperature was assumed to be constant at 70 °C. An adapted equation for the heat-transfer coefficient for a thermally and hydrodynamically developing entrance region was applied to calculate the temperature profile.[22] Figure 6 shows the calculated bulk flow temperature profile inside one heat-exchanger tube, using an inlet temperature of 1000 °C. The inlet velocity, necessary for calculating the heat-transfer coefficient in one heat-exchanger tube, was calculated in such a way that the velocity in the measurement section downstream of the heat exchanger was approximately 6 m/s. From Figure 6, it can be observed that the calculated outlet temperatures for both tube diameters are below 200 °C, satisfying the boundary conditions described. Conservation of mass, in combination with temperature-dependent physical properties is applied to calculate the Reynolds number. From Figure 7, an increasing Reynolds number can be observed with a decreasing flue gas temperature; however, the flow is always laminar, indicated by Re < 2300. The pressure drop over the heat exchanger is depicted in Figure 8. For both tube diameters, the maximum pressure drop is always below 350 Pa.

4.2.2. Compact Laminar Counterflow Gas to Gas Heat Exchanger. From Figure 3, it can be observed that an equivalent tube diameter of approximately 2 mm could result in a significant decrease of the aerosol emissions. However, manufacturing a shell and tube heat exchanger with a tube diameter of approximately 2

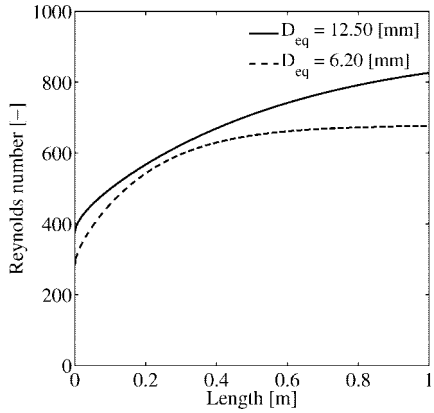

Figure 7. Calculated Reynolds number for two different tube dimensions as a function of the length for the water-cooled heat exchanger.

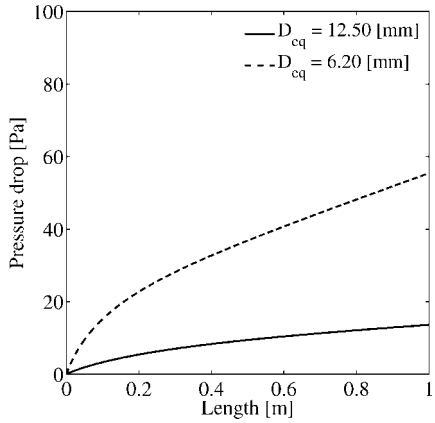

Figure 8. Calculated pressure drop for two different tube dimensions as a function of the length for the water-cooled heat exchanger.

mm is very expensive and labor-intensive. Sealing problems, in combination with a lot of small and short tubes, which are required not to exceed the maximum pressure drop over the heat exchanger, have led to an alternative design.

Although water is commonly employed as cooling medium in biomass combustion plants, air is also preheated by flue gases in a number of applications. Using air instead of water as a cooling medium gives the opportunity to use a compact laminar counterflow gas to gas heat exchanger, originally developed for recuperative burners.[21] This heat exchanger with an equivalent tube diameter of 2.22 mm is made of heat-resistant stainless steel. To obtain a sufficient heat-exchanging surface, the heat exchanger is constructed as a counterflow heat exchanger in between two halves of a cross-flow heat exchanger. Furthermore, the plates are manufactured in a way that each cooling channel is in full in contact with a flue gas channel. A scheme of the compact laminar counterflow gas to gas heat exchanger is depicted in Figure 9.

The flue gas inlet of the heat exchanger is connected with the secondary combustion zone of the pilot-scale furnace. A directly adjustable mass flow controller with a maximum capacity of 1.25 N m^3 min^{-1} (not shown in Figure 9) is used to achieve a constant mass flow of the cooling air through the gas to gas heat exchanger. The hot cooling air is freely exhausted. The ducts are isosceles triangles with a base of 6 mm and a height of 2.5 mm. The channels depicted in Figure 9 are drawn as square ducts to illustrate the countercurrent flow concept of this gas to gas heat exchanger. The equivalent diameter of one of the channels of the gas to gas heat exchanger is 2.22 mm. Each row of the gas to gas heat exchanger consists of 28 channels, whereas the number of rows is 75. The connection of the channels and the housing on both sides of the heat exchanger is accomplished by a header, which consists of a three-dimensional structure. The effective length of the heat exchanger is 100 mm, whereas the maximum entrance length of

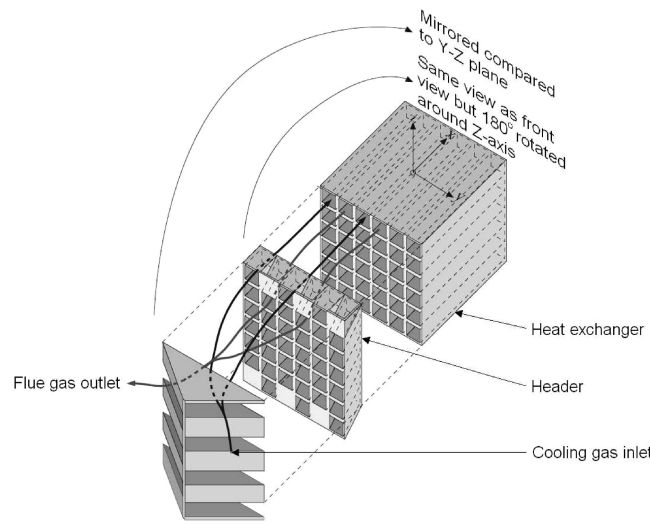

Figure 9. Schematic picture of the used gas to gas heat exchanger, originally developed to transfer 20 kW of heat.

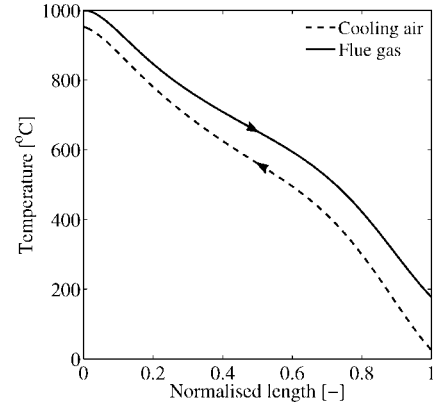

Figure 10. Calculated flue gas and cooling air temperature in the gas to gas heat exchanger as a function of the normalized length.

the header on the furnace side is 55 mm. The exit length of the header (not drawn in Figure 9) varies because of the complex geometry between 4 and 130 mm.

For the calculations, it is assumed that the heat capacity flows $\dot{m}_{cp}$ for both gas flows are equal. A fully developed hydrodynamic and thermodynamic flow are assumed for the calculation of the heat-transfer coefficient, which is in contradiction to the calculation of the heat-transfer coefficient for the water-cooled heat exchanger. This assumption is valid because of the fact that the entrance length of both phenomena is much smaller compared to the total length of the heat exchanger. In the case of gases when the Prandtl number is around 0.7, the flow develops thermally more rapidly than it does hydrodynamically. From this point of view, the hydrodynamic entrance length is the only relevant parameter with respect to the entrance length, which is expressed by[13]

$$\frac{z_e}{D_{eq}} \simeq 0.05\mathrm{Re} \tag{13}$$

where z_e represents the hydrodynamic entrance length. An estimation of the Reynolds number is made by first calculating the temperature profile by neglecting the entrance effects and applying conservation of mass. Substituting the maximum Reynolds number in eq 13 gives a worst-case indication of the hydrodynamic entrance length (explained later on).

Figure 10 shows the calculated temperature profile of both the flue gas and the cooling air flow as a function of the normalized length by neglecting the entrance region. For the calculations, an initial flue gas temperature and an initial cooling air temperature of 1000 and 20 °C, respectively, are assumed. The initial flue gas

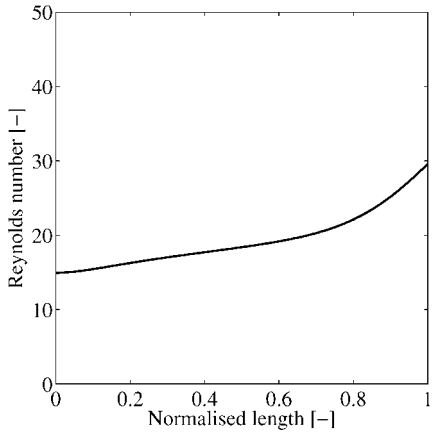

Figure 11. Calculated Reynolds number of the flue gas in one channel of the gas to gas heat exchanger as a function of the normalized length.

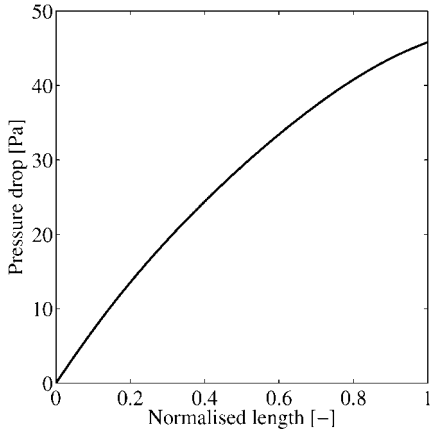

Figure 12. Calculated pressure drop of the flue gas in one channel of the gas to gas heat exchanger as a function of the normalized length.

velocity was set to 6 m/s in the measurement section. From Figure 10, it can be observed that the calculated outlet temperature of the flue gas should be lower than 200 °C, which should be sufficient to complete the condensation process. The Reynolds number expressed in Figure 11 was calculated by applying conservation of mass, in combination with temperature-dependent physical properties of the flue gas. From Figure 11, a maximum Reynolds number of approximately 30 can be observed. Substituting this Reynolds number in combination with an equivalent tube diameter of 2.22 mm in eq 13 yields a maximum entrance length of less than 4 mm, which is much smaller compared to the total length of the heat exchanger. Therefore, it is proven that the assumption of neglecting the entrance effects is valid. Figure 12 shows the calculated pressure drop over the gas to gas heat exchanger, which was always below 350 Pa.

5. Results and Discussion

The setup as shown in Figure 4 is used to investigate the influence of the three different heat-exchanger designs on the particulate emissions. Impactor measurements to determine the particle size distribution (PSD) after both the specially designed heat exchangers and the boiler were performed at almost the same time. Flue gas temperatures, oxygen contents, and velocities were recorded during the test runs.

Chemically untreated wood chips with a typical dimension of a couple of centimeters are chosen as a fuel for all experiments. The fuel used for the experiments is stored in a container with a limited capacity. Several fuel batchs were required for the experiments; however, for each heat-exchanger design, the same fuel batch was used. Using different fuel batches results in slightly varying amounts of aerosol-forming species, such as K, Cl, S, Pb, Na, and Zn. Consequently, the potential for aerosol formation also changes for each fuel batch. Therefore, the amount of aerosol-forming elements in the fuel is analyzed. On the other hand, process control parameters, such as oxygen content, load capacity, and consequently, flue gas velocities also change for different fuel compositions because of slightly varying heating values, moisture contents, and flue gas compositions. Because of this, a distinction between the three heat-exchanger designs is made, indicated with case 1 for the water-cooled heat exchanger with an equivalent tube diameter of 12.50 mm, case 2 for the water-cooled heat exchanger with an equivalent tube diameter of 6.20 mm, and case 3 for the gas to gas heat exchanger with an equivalent tube diameter of 2.22 mm.

Table 1. Composition Wood Chips Used for the Experiments[a]

parameter	unit	case 1 average value	case 2 average value
moisture	wt % (wb)[b]	29.2 ± 7.8	27.8 ± 1.8
ash	wt % (db)	1.4 ± 0.6	0.9 ± 0.1
S	mg/kg (db)	166.0 ± 39.0	134.0 ± 4.9
Cl	mg/kg (db)	99.7 ± 52.3	80.0 ± 5.8
Si	mg/kg (db)	1028.3 ± 708.7	528.8 ± 479.4
Na	mg/kg (db)	100.3 ± 0.6	21.4 ± 6.3
Mg	mg/kg (db)	312.3 ± 114.1	270.0 ± 16.9
K	mg/kg (db)	929.7 ± 336.6	757.8 ± 118.7
Ca	mg/kg (db)	3062.7 ± 1019.9	2251.0 ± 364.3
Zn	mg/kg (db)	20 ± 19.1	7.6 ± 5.1
Pb	mg/kg (db)	<10[c]	14.0 ± 5.5

[a] Explanation: case 1, water-cooled heat exchanger with D_{eq} = 12.50 mm; case 2, water-cooled heat exchanger with D_{eq} = 6.20 mm. [b] wb, wet base; db, dry base. [c] Below detection limit.

Table 1 contains information regarding the moisture content as well as the ash content and the concentrations of the most relevant ash and aerosol-forming elements of the fuel applied for each case. Unfortunately, no fuel analysis was available regarding case 3. From Table 1, it can be observed that there are some significant differences in the fuel composition. The amount of sodium in case 1 for instance is significantly higher compared to case 2. Furthermore, on average, the amount of potassium in the fuel for case 1 is higher compared to case 2; however, because of the strong deviations, this difference is not significant.

On the basis of a fuel analysis, a gas to particle conversion can be made. If 100% of all K, Cl, S, Pb, Na, and Zn is volatilized and released to the gas phase, than a theoretical aerosol concentration of 174.8 and 131.0 mg N^{-1} m^{-3} can be achieved for cases 1 and 2, respectively. Dependent upon the S and Cl content, most of the K and Na are bound as chlorides and sulfates. In case of an excess of K and Na, these elements can also bound as carbonates. Against it, Zn and Pb are mainly bound as oxides. However, in general, a total release rate of 100% could hardly be achieved in practical situations; therefore, the amount of particulate-forming species in the flue gas is lower. In general, a high release of Cl, S, Zn, and Pb up to 80−100% is observed at temperatures above 850 °C.[10,14,16] K and Na are both released at rather low release rates. Na is found to be released at approximately 30%, whereas approximately 35−70% of K is released to the gas phase at a combustion

(14) Jensen, P. A.; Frandsen, F. J.; Dam-Johansen, K.; Sander, B. *Energy Fuels* **2000**, *14*, 1280–1285.
(15) Jöller, M.; Brunner, T.; Obernberger, I. *Energy Fuels* **2005**, *19*, 311–323.
(16) Knudsen, J. N.; Jensen, P. A.; Dam-Johansen, K. *Energy Fuels* **2004**, *18*, 1385–1399.

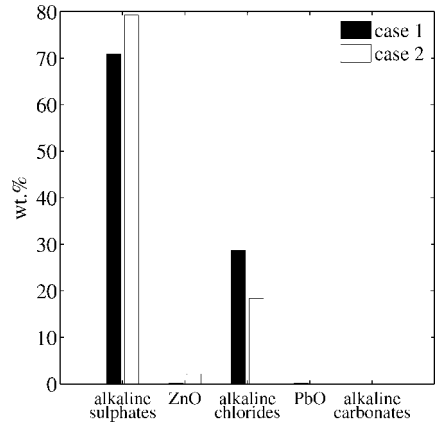

Figure 13. Aerosol composition calculated from the elemental composition. Explanation: case 1, water-cooled heat exchanger with $D_{eq} = 12.50$ mm; case 2, water-cooled heat exchanger with $D_{eq} = 6.20$ mm.

temperature of 1000 °C.[10,16] This, in combination with a substantial share of potassium in the fuel, indicates that the total amount of particulate-forming species in the flue gas is significantly lower compared to that theoretical expected.

Calculations showed that the total amount of particle-forming species in the flue gas for case 1 is of about 75 mg N^{-1} m^{-3}. The composition of the aerosol emissions, calculated from the fuel composition, showed that almost 80 wt % consists of alkaline sulfates. Besides alkaline sulfates, also a large share of alkaline chloride can be found in the aerosols for case 1, more than 18 wt %. The remaining small part mainly consists of ZnO (≈2 wt %) and a small share of PbO and alkaline carbonates. A graphical representation of the aerosol composition based the fuel analysis for case 1 is represented in Figure 13.

From the gas to particle conversion, it can be observed that the total amount of aerosol-forming species in the flue for case 2 is almost 58 mg N^{-1} m^{-3}, from which 75 wt % consists of alkaline sulfates and 21 wt % consists of alkaline chlorides. Furthermore, it is expected that the aerosols for case 2 also contain some small shares of PbO and ZnO, 2.2 and 1.1 wt %, respectively.

A steady-state temperature distribution inside the furnace was required during the BLPI measurements. A quite stable temperature of approximately 1000 °C could be achieved in the secondary combustion zone T_{sec} during the impactor measurement downstream of the heat exchanger and the boiler for cases 2 and 3. The flue gas temperatures in the secondary combustion zone for case 1 were slightly lower during the impactor measurements downstream of the test heat exchanger and the ordinary boiler. However, it is expected that the flue gas temperatures in the secondary combustion zone during all

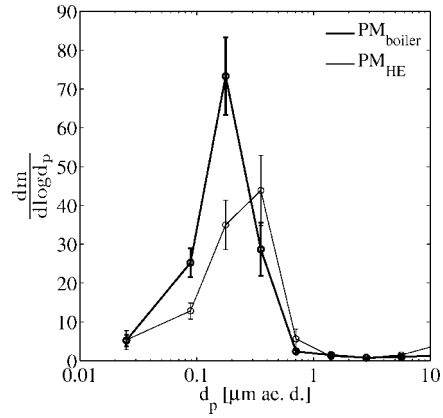

Figure 14. Case 1: typical particle size distributions, determined with a nine-stage Berner-type low-pressure impactor (BLPI) downstream of the ordinary boiler and the heat-exchanger outlet, with an equivalent tube diameter of 12.50 mm, denoted with the subscripts boiler and HE, respectively, values in mg Nm^{-3} related to 13 vol % O_2. Explanation: ae. d., aerodynamic particle diameter.

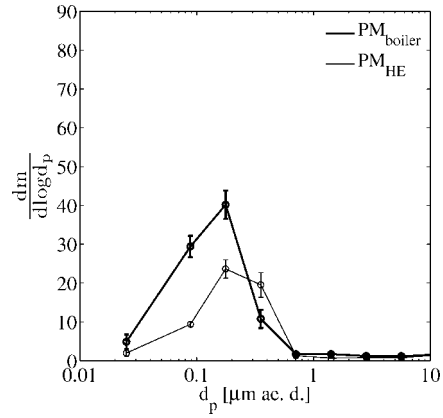

Figure 15. Case 2: typical particle size distributions, determined with a nine-stage Berner-type low-pressure impactor (BLPI) downstream of the ordinary boiler and the heat-exchanger outlet, with an equivalent tube diameter of 6.20 mm, denoted with the subscripts boiler and HE, respectively, values in mg Nm^{-3} related to 13 vol % O_2. Explanation: ae. d., aerodynamic particle diameter.

impactor measurements should be sufficient to avoid major particle formation before the heat-exchanger inlet.

When the measured flue gas temperatures downstream of the water-cooled heat exchangers were compared (cases 1 and 2), a rather good agreement between the measured and theoretically determined flue gas temperatures can be observed (see Figure 6). Deviations between the theoretical determined flue gas temperature and the measured flue gas temperature near the outlet of the gas to gas heat exchanger (case 3) are caused by the fact that the gas to gas heat exchanger originally is developed to transfer 20 kW of heat, whereas the heat transferred during the experiments was limited at approximately 7.5 kW. Therefore, the gas to gas heat exchanger was not well-balanced, which results in lower flue gas temperatures at the outlet.

BLPI measurements downstream of the three heat exchangers tested as well as downstream of the ordinary boiler have been performed. The average particle size distributions for the different cases are depicted in Figures 14−16. The average PSD for case 1 is based on 13 repetitive BLPI measurements, whereas 26 BLPI impactor measurements have been performed to determine the average PSD for case 2. With regard to case 3, only 6 repetitive measurements have been performed. From Figures 14−16, it can be observed that the PSD downstream of the heat exchangers tested as well as downstream of the boiler

(17) van Loo S.; Koppejan, J. *Handbook of Biomass Combustion and Co-firing*; Twente University Press: Enschede, The Netherlands, 2002.
(18) Obernberger, I.; Brunner, T.; Jöller, M. In Proceedings of the IEA Seminar Aerosols from Biomass Combustion; Nussbaumer, T., Ed.; Verenum: Zürich, Switserland, 2001; pp 69–74.
(19) Seinfeld, J. H. *Atmospheric Chemistry and Physics of Air Pollution*; John Wiley and Sons, Inc.: New York, 1986.
(20) van Kemenade H. P. In *Aerosol in Biomass Combustion*; Obernberger, I., Ed.; Medienfabrik Graz: Graz, Austria, 2005; pp 107–118.
(21) van Kemenade, H. P. In *Innovative Process Design*; Eindhoven University of Technology: Eindhoven, The Netherlands, 2006; ISBN 978-90-386-2928-5.
(22) Verein Deutscher Ingenieure (VDI). *Wärmeatlas*, 6th ed.; VDI-Verlag GmbH: Düsseldorf, Germany, 1991.
(23) Valmari, T.; Kaupinnen, E. I.; Kurkela, J.; Jokiniemi, J. K.; Sfiris, G.; Revitzer, H. *J. Aerosol Sci.* **1998**, *294*, 445–459.

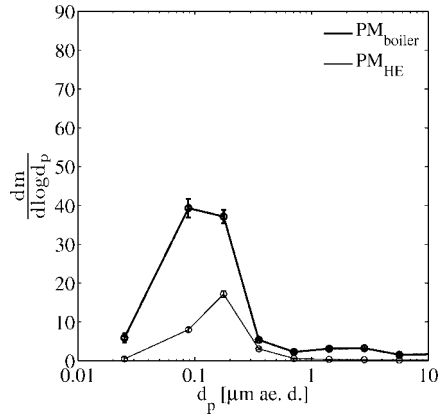

Figure 16. Case 3: typical particle size distributions, determined with a nine-stage Berner-type low-pressure impactor (BLPI) downstream of the ordinary boiler and the heat-exchanger outlet, with an equivalent tube diameter of 2.22 mm, denoted with the subscripts boiler and HE, respectively, values in mg Nm^{-3} related to 13 vol % O_2. Explanation: ae. d., aerodynamic particle diameter.

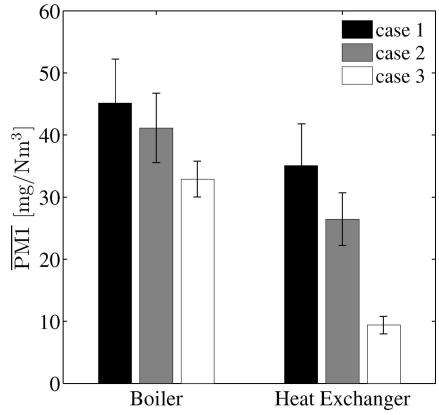

Figure 17. Average fine particulate emission PMI (mg N^{-1} m^{-3}) downstream of boiler and heat exchanger tested. Explanation: case 1, water-cooled heat exchanger with $D_{eq} = 12.50$ mm; case 2, water-cooled heat exchanger with $D_{eq} = 6.20$ mm; case 3, gas to gas heat exchanger with $D_{eq} = 2.22$ mm.

always shows one clear peak that is usually around the third and fourth stage (cut diameter of 0.25 and 0.5 μm, respectively). When the PSD from cases 1 and 2 was compared to the fuel analysis as shown in Table 1, then it can be observed that the higher the amount of aerosol-forming elements in the fuel, the higher the amount of aerosols formed.

For case 3, a remarkable trend can be observed regarding the PSD at larger cut diameters. At larger cut diameters, a small share of particles can be observed downstream of the boiler, whereas almost no particles can be observed at these cut diameters downstream of the heat exchanger tested; this is contrary to what is observed for cases 1 and 2. A possible explanation for this trend can be found that, because of the complex geometry in combination with small channels, a part of these relatively large particles will end up in the corners of the heat exchanger as a result of inertia effects. Furthermore, thermophoresis can be of importance when applying small channel dimensions with relatively large temperature gradients; however, this is a topic of further investigation.

From Figure 17, it can be seen that the average normalized particle fraction with an aerodynamic diameter <1 μm, downstream of the boiler $PM1_{boiler}$ for cases 1 and 2 were 45.15 and 41.16 mg N^{-1} m^{-3}, respectively, which is equal to within the statistical accuracy. For case 3, a slightly lower average particulate emission after the boiler of 34.88 mg Nm^{-3} was

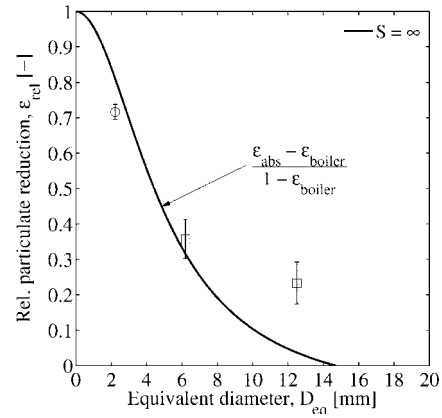

Figure 18. Theoretical (continuous and dashed line) and measured (○, gas to gas heat exchanger; □, water-cooled heat exchanger) particulate emission reductions compared to emissions of plants with an ordinary boiler design ($\epsilon_{boiler} = 10\%$). Measured particulate emission reductions are determined with a 95% confidence interval.

observed. The particle fraction with an aerodynamic diameter <1 μm, downstream of the heat exchanger $PM1_{HE}$ shows, of course, a strong decreasing trend while decreasing the tube diameter of the heat exchanger. However, this finding was already predicted from Figure 18; decreasing the tube diameter results in less particulate emissions.

With the coupled set of impactor measurements performed downstream of the heat exchanger tested and the boiler, it is possible to determine a statistically proven PM1 emission reduction. The average relative particulate emission reductions related to the ordinary boiler design $\epsilon_{rel,exp}$ was calculated according to the following relation:

$$\overline{\epsilon_{rel,exp}} = \frac{1}{n}\sum_{i=1}^{n}\left(1 - \frac{PM1_{test,i}}{PM1_{boiler,i}}\right) \qquad (14)$$

In eq 14, $PM1_{test,i}$ and $PM1_{boiler,i}$ represents the normalized particle fraction with an aerodynamic diameter <1 μm of one coupled set of measurements expressed in mg Nm^{-3} related to dry flue gas (13 vol % O_2). The subscripts test and boiler referred to the test heat exchanger and the ordinary boiler, respectively. The number of coupled sets of measurements performed for each test heat-exchanger dimension is represented by n. It is noticed that, because the average particulate emission reduction is nonlinear in the input parameters, the calculated average relative particulate emission reductions, $\epsilon_{rel,exp}(PM1_{test}, PM1_{boiler})$, is not equal to $\epsilon_{rel,exp}(PM1_{test}, PM1_{boiler})$.

The average relative particulate emission reductions $\epsilon_{rel,exp}$ obtained with the three different heat exchangers are depicted in Figure 19. From Figure 18, it can clearly be seen that decreasing the tube diameter results in an increase of the average relative particulate emission reduction. This reduction increases from 23 $\pm$ 6.4% using a tube diameter of 12.50 mm (case 1) up to 72 $\pm$ 2.1% using a tube diameter of 2.22 mm (case 3). All data are related to dry flue gas, 13 vol % O_2, determined with a 95% confidence interval. Consequently, stimulating condensation of aerosol-forming species results in a rapid builtup of the fouling layer inside the heat exchanger. Visual inspection of the fouling layer showed a nonsticky powdery condensation layer that could easily be removed by applying pressurized air. Blocking of the heat exchanger with coarse fly ash particles during the experiments was prevented as a result of the fact that a major part of the coarse fly ash particles was captured in the secondary combustion zone by inertia effects.[20] In real small-scale biomass combustion units, the flue gas velocities in the

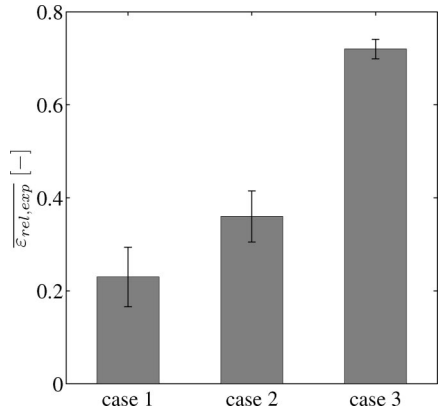

Figure 19. Overview of the average particulate emission reduction, related to dry flue gas, 13 vol % O_2. Explanation: case 1, water-cooled heat exchanger with D_{eq} = 12.50 mm; case 2, water-cooled heat exchanger with D_{eq} = 6.20 mm; case 3, gas to gas heat exchanger with D_{eq} = 2.22 mm.

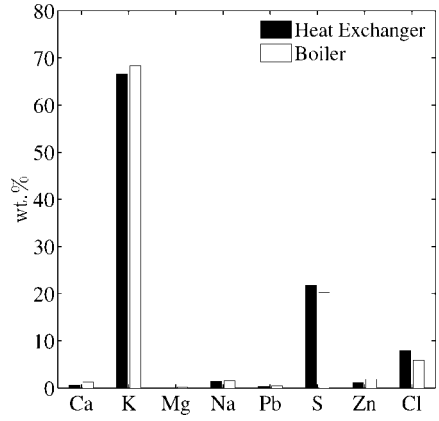

Figure 20. Comparison of the chemical composition of aerosols downstream of the heat exchanger and boiler.

furnace are lower and, therefore, the concentrations of coarse particles will also be smaller; thus, major problems caused by the coarse fly ash particles in real applications are not expected.

Wet chemical analysis of BLPI foils have been performed to obtain insight into whether the heat-exchanger design effected the chemical composition of the aerosols formed. The results of the chemical analysis presented in Figure 20 are based on one impactor measurement downstream of the heat exchanger tested and the boiler. From this figure, it can be observed that the heat-exchanger design hardly influences the chemical composition of the aerosol formed. Furthermore, it can be observed that the aerosols formed mainly consist of K and S. Because of this, the assumption that K_2SO_4 is the main aerosol component is once more confirmed.

To check if the trend of the competing processes described in section 3 are correct, simulations of the absolute particulate emission reductions have been performed, which are compared to the measurement results. To perform a worst-case simulation, calculations regarding the wall condensation rate with an infinite saturation ratio S have been performed. The background for this assumption is that, for an infinite saturation ratio S, the lowest wall condensation rate can be obtained (see Figure 3).

To make the measurement results comparable to what is theoretically expected, losses of aerosols and aerosol-forming vapors on the surfaces of the boiler, which are expected to be in the range of 10%, have to be considered (see van Kemenade).[20] Consequently, the theoretical absolute particulate emission reduction, calculated by eq 12, is always higher compared to the relative particulate emission reduction obtained by the experiments. Because of this, a relation between the theoretical relative particulate emission reduction and the theoretical absolute particulate emission reduction is given, such that the measurement results could be compared to what is theoretically expected. This relation is defined as

$$\epsilon_{rel,theo} = \frac{\epsilon_{abs,theo} - \epsilon_{boiler}}{1 - \epsilon_{boiler}} \quad (15)$$

where $\epsilon_{rel,theo}$ represents the theoretical relative particulate emission reduction. The absolute amount of aerosols and aerosol-forming species that end up in the fire tube and boiler are represented by ϵ_{boiler}. From Figure 18, it can be observed that the predicted trend of the theoretical determined particulate emission reduction is in agreement with the measured particulate emissions.

The approach as described in section 3 shows good agreement with the results obtained with the measurements; decreasing the tube diameter indeed results in a reduction of the fine particulate emissions. As stated in section 2, additional particle deposition mechanisms, such as thermophoresis, coagulation, and Brownian motion, seem to be secondary effects regarding the particle emission reduction. Nevertheless, the effect of thermophoresis on the particle deposition rate could be of importance, especially for submicrometer particles in small tubes with strong temperature gradients; however, this is a subject of further investigation. Furthermore, in the theoretical approach, it is assumed that the aerosol-forming species, which are already transformed into particles before they will enter the heat exchanger, will not contribute in the wall condensation rate. This is of coarse true for calculating the wall condensation rate; however, a certain amount of these particles cannot (or partially) be separated from the flue gas. These particles still cause some fine particulate emissions downstream of the heat exchangers tested, especially for the heat exchangers with relatively small flue gas passages.

6. Summary and Conclusions

An analytical approach that incorporates heterogeneous condensation and wall condensation is derived to investigate whether there is a physical basis for condensation of aerosol-forming elements on heat-exchanger walls by preference. Consequently, stimulating wall condensation results in fine particulate emission reductions to the atmosphere. Continuum diffusion of molecules toward already present nuclei in the flue gas in combination with a correction factor for diffusion outside the continuum limit is used in the approach. This approach indicates a significant reduction of aerosol emissions by preference of wall condensation when a sufficient heat-exchanging area is provided; the distance to the wall in every cross-section is in the millimeter range, and the flow regime is laminar. This approach has been tested on a pilot-scale biomass combustion plant. A slip stream was extracted from the secondary combustion zone and fed to two tubular water-cooled heat exchangers and one triangular-shaped gas to gas heat exchanger, respectively, both exhibiting typical equivalent tube diameters in the millimeter regime and Reynolds numbers up to 1000.

The trend of the approach derived is a conservative one and showed a good agreement with the measurement results. Measurements show that a reduction in the particulate emission related to ordinary boiler designs of more than 70% could be achieved using a gas to gas heat exchanger with an equivalent diameter of 2.22 mm, which is a significant difference. Additional particle and vapor deposition mechanisms neglected are

seemingly of second-order effect and are therefore not relevant for providing guidelines regarding the design of an aerosol-reducing heat exchanger. However, the influence of thermophoresis is a subject that is still a topic of further investigation.

Besides measurements regarding aerosol precipitation efficiencies, also, a gas to particle conversion based on a fuel analysis and release rates obtained from the literature have been performed. From the analysis, it could be observed that almost 75 wt % of the aerosols formed should consist of alkaline sulfates. Furthermore, also, a wet chemical analysis of the aerosol compositions downstream of the heat exchanger tested and the boiler have been performed. The wet chemical analysis showed that the influence of the heat exchanger design on the chemical aerosol composition does not have an significantly noticeable effect. Moreover, it could also be observed that the aerosols formed indeed mainly consist of potassium and sulfur.

For the future outlook, it is expected that the demands regarding the fine particulate emissions PM1 for small-scale biomass combustion units will be sharpened by the government. Then, the relevance of a new cost-efficient aerosol precipitation technique becomes of more importance. Because of this, a start is made toward a simple and cheap aerosol precipitation technique. The gas to gas heat exchanger presented is a good start but is, because of its complex geometry, expensive to produce, whereas the practical applicability is of minor interest in small-scale biomass combustion plants. Therefore, an adapted heat-exchanger design has to be developed that is able to heat up water by use of small flue gas passages. The resulting heat-exchanger design should be akin to compact designs used in, for instance, the aircraft and air-conditioning industry. These heat exchangers are able to transfer heat from a gaseous medium toward a liquid, in combination with small-channel passages. Besides this, such heat exchangers also exhibit a good optical accessibility, which enables the use of simple heat-exchanging cleaning systems. Further research is required with regard to the behavior of the deposition layer buildup to develop suitable heat-exchanger cleaning systems.

Acknowledgment. The authors thank Level Energietechniek, Son, The Netherlands, for making the compact laminar counterflow gas to gas heat exchanger available. Furthermore, the financial support of the Austrian K-plus program is gratefully acknowledged.

EF060435T